



# Estimation of seafloor reflectivity in shallow water based on seismic data of sparker sources

Jianglong Zheng<sup>1,2,3</sup> · Jiang Xu<sup>2</sup> · Siyou Tong<sup>1</sup> · Yifan Huang<sup>3</sup> · Huawei Zhou<sup>1,4</sup>

Received: 28 October 2020 / Accepted: 19 September 2021 / Published online: 29 September 2021  
© The Author(s), under exclusive licence to Springer Nature B.V. 2021

## Abstract

Seafloor acoustic reflectivity is fundamental for both underwater detection and ocean acoustic field prediction, especially in shallow-water offshore regions. This paper presents a procedure to estimate the seafloor reflectivity in shallow water based on the direct wave and seafloor reflection data from single-channel seismic records of sparker sources. We apply the procedure to a seismic line acquired in the western part of the Taiwan Strait. To resolve the uncertainty in the inversion results, we implement strict quality control on the data obtained from seismic records and utilized for the inversion calculation. According to the preprocessing results, it is recommended to exclude the bubble pulses and their surface reflections, which are unstable and act as noise, from the estimated source wavelet applied to the inversion calculation. The calculation results show a significant level of directional variation in the acoustic energy radiated from the sparker source, and this variation should be considered in the calculation of seafloor reflectivity. In this work, the seafloor reflectivity is calibrated with relatively stable calculated values that correspond to known types of sediment, and the directivity constant of a sparker source is estimated ( $\approx 0.2$ ), which is defined as the amplitude ratio between horizontally propagating seismic waves and vertically propagating seismic waves. The resulting relationship between the seafloor reflectivity and the sediment type is consistent with those of previous research, indicating the feasibility of our procedure.

**Keywords** Seafloor reflectivity · Direct wave · Sparker · Sediment classification

## Introduction

The acoustic properties of the seabed are critical for seabed detection and underwater acoustic propagation (e.g., Kibblewhite 1989; Vardy 2017; Wan et al. 2010). Measurement techniques for obtaining the acoustic properties of sediment can be classified into direct measurements (e.g., via sediment probes, sediment cores, and laboratory studies) that are typically obtained at high frequencies,  $O(10^4\text{--}10^5)$  Hz (e.g., Endler et al. 2015; Hamilton 1970; Hou et al. 2018; Kim et al. 2012; Tian et al. 2019; Wang et al. 2016), and indirect

measurements, the acoustic parameters of which are inferred from long-range propagation or reflection data (e.g. Holland and Dosso 2013; Liu et al. 2016, 2020; Schock 2004a, b; Vardy 2015), generally  $O(10^2\text{--}10^4)$  Hz. While indirect measurements are cost-effective and offer broad prospects, however, the need to resolve the uncertainty in the inversion results remains a fundamental challenge (Dettmer et al. 2007, 2013).

Subbottom profiling is an important approach for offshore marine geological seismic surveying, and many studies in the literature have successfully used subbottom profile data (chirp source) to invert the seafloor acoustic parameters (e.g., Chiu et al. 2015; Rakotonarivo et al. 2011; Schock et al. 1989; Stevenson et al. 2002; Schock 2004a, b; Tseng et al. 2012; Zheng et al. 2019). The widespread use of the chirp compression pulse technology is largely due to its stable acoustic signature. The inversion results of the chirp data provide the response characteristics of the seafloor to the pulsed acoustic waves with a center frequency of several kilohertz. Sparkers, including underwater plasma sources, are another seismic source that are widely employed and are

✉ Jianglong Zheng  
jl.zheng@siat.ac.cn

<sup>1</sup> Ocean University of China, Qingdao, China

<sup>2</sup> Third Institute of Oceanography, Ministry of Natural Resources, Xiamen, China

<sup>3</sup> Shenzhen Institute of Advanced Technology, Chinese Academy of Sciences, Shenzhen, China

<sup>4</sup> University of Houston, Houston, TX, USA

controllable and repeatable to a certain extent. The inversion of sparker data can provide the response characteristics of the seafloor to pulsed acoustic waves with a center frequency of several hundred hertz (e.g., Duchesne et al. 2007).

Estimating seafloor reflectivity is usually a routine step in acoustic inversion, the results of which can be directly employed as parameters for the acoustic classification of seafloor sediments (e.g., Breslau 1964; Faas 1969; Parrott et al. 1980; Smith and Li 1966; Stoll and Kan 1981; Tyce 1976) or as input parameters for the estimation of other seafloor properties (Chiu et al. 2015; Chotiros et al. 2002; Heard 1997; Schock 2004a, b; Zheng et al. 2012). Many studies on the inversion of seafloor parameters based on chirp data can be used for reference; some of these studies are mentioned in this paper. However, the seafloor reflectivity calculation method commonly applied to the inversion of chirp data may be invalid when applied to seismic data acquired in shallow water areas, especially to seismic data with a lower-frequency seismic source, similar to the problems encountered in our actual applications of sparker data. The early work with an explosive source or underwater discharge usually estimated reflectivity based on direct arrival and reflected waves; however, details of the key parameters were not available (e.g., Hastrup 1969; Parrott et al. 1980), and the method is not applicable to single-channel seismic data at sea. Therefore, details of the inversion calculation must be different for seismic data obtained using different types of seismic sources and acquisition geometries.

A marine sparker source works based on the shock wave effect of an underwater electric discharge. This underwater discharge creates a high-pressure plasma/vapor bubble in water, and the oscillations of this bubble generate an acoustic signature similar to the signatures generated by air guns and underwater explosions. Most current underwater sparkers work based on the corona discharge principle with multiple electrodes in the transmitting terminal. According to studies of underwater discharges (e.g., Buogo et al. 2009; Cook et al. 1997; Huang et al. 2014, 2015, 2016), the acoustic signature of multi-electrode sparkers is determined

by the discharge energy of each single electrode, number of electrodes, spacing between electrodes and physical properties of seawater.

Generally, sparker sources are placed immediately beneath the sea surface (usually approximately 1 m) during field data acquisition. Therefore, the acoustic signature of a sparker source, including the primary pulse and bubble pulses (Fig. 1), is also influenced by the dynamic changes in the seawater surface. Due to their direct dependency on the discharge process, the primary pulse and its surface reflection should be mostly stable. In contrast, the bubble pulses should be more unstable due to the combined effect of the bubble properties, the bubble oscillating process and their mutual influence, and the surrounding seawater environment. The characteristics of the pressure waves generated by sparker sources and the sea surface are important for seismic data processing, inversion, and interpretation of the corresponding data.

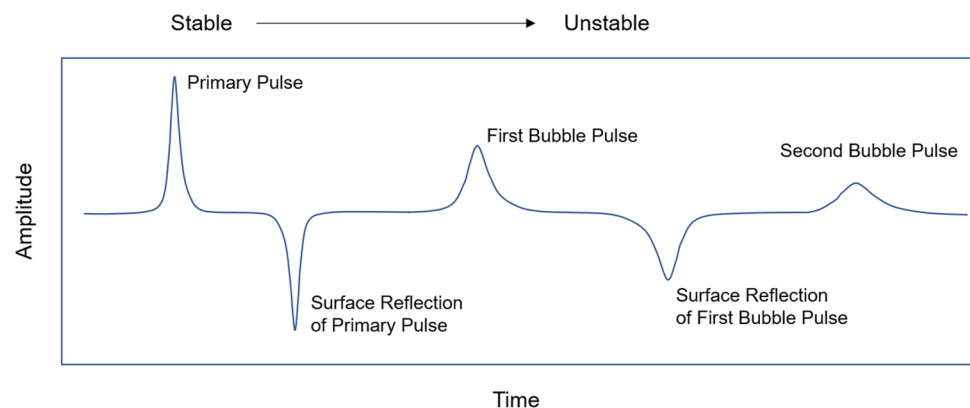
This paper focuses on deducing the seafloor reflectivity from sparker data with a case study considering the working principle of sparker sources and the actual data acquisition environment while applying a novel approach. The inversion results based on sparker data constitute an important supplement to the study of the acoustic properties of the seafloor at the low-frequency end.

## Methods

### Estimating seafloor reflectivity using primary and secondary seafloor reflections

The seafloor reflectivity is usually denoted in terms of the reflection coefficient or reflection loss; the latter can show a larger dynamic range. In this work, we use reflectivity when describing general seafloor properties, and when presenting the exact calculated values, we use the reflection coefficient or reflection loss. Estimating the seafloor reflection coefficient is an important step for sediment inversion using

**Fig. 1** Schematic of pressure waves generated by an underwater sparker source and the sea surface



reflection seismic data. According to previous studies (e.g., Bull et al. 1998; Chiu et al. 2015; Schock 2004b; Zheng et al. 2012), the seafloor reflection coefficient can be calculated based on the ratio between the primary and secondary seafloor reflections and their corresponding two-way travel times from normally incident reflection data:

$$RC = \frac{A_s}{A_p} \times \frac{T_s}{T_p} \tag{1}$$

where  $RC$  represents the normal-incidence reflection coefficient of the seafloor;  $A_p$  and  $A_s$  are the amplitudes of the primary and secondary reflections, respectively, from the seafloor; and  $T_p$  and  $T_s$  are the corresponding two-way travel times. The two-way travel time in this equation compensates for the impact of spherical spreading on the amplitudes. Here, the reflection coefficient of the air-water interface is assumed to be  $-1$ , which means that the amplitude difference between the secondary and primary reflections is due to the occurrence of additional seafloor reflections, as shown in Fig. 2.

The equation also assumes that the primary and secondary seafloor reflection data have sufficiently high signal-to-noise ratios. This assumption is reasonable for chirp data in sufficiently deep water but less accurate for seismic data acquired in shallow water or with a lower-frequency seismic source, in which the transmitted wave overlaps with the reflections. The latter case can be explained by the following equation:

$$RC_{calculate} = \frac{A_s + A_x}{A_p} \times \frac{T_s}{T_p} = RC_{seafloor} + \frac{A_x}{A_p} \times \frac{T_s}{T_p} \tag{2}$$

where  $RC_{calculate}$  represents the calculated reflection coefficient;  $A_x$  represents the amplitude of reflections from any strata below the seafloor or noise, which is usually unpredictable; and  $RC_{seafloor}$  represents the seafloor reflection coefficient that we aim to calculate.

Hence, the results of the seafloor reflection coefficient calculation would be unreasonable in the case of a significant level of noise or additional reflections that overlap

with the secondary reflections. Unfortunately, it is nearly impossible to remove additional reflections that are usually unknown. Hence, it is necessary to find new ways for calculating seafloor reflection in shallow water, similar to the method proposed in this study.

### Estimating seafloor reflectivity using the direct wave and primary seafloor reflection

Theoretically, the reflection coefficient of the target layer can be calculated based on normally incident and reflected waves:

$$RC = \frac{A_r}{A_i} \tag{3}$$

where  $A_r$  is the amplitude of the reflected wave and  $A_i$  is the amplitude of the incident wave on a layer, such as the seafloor.

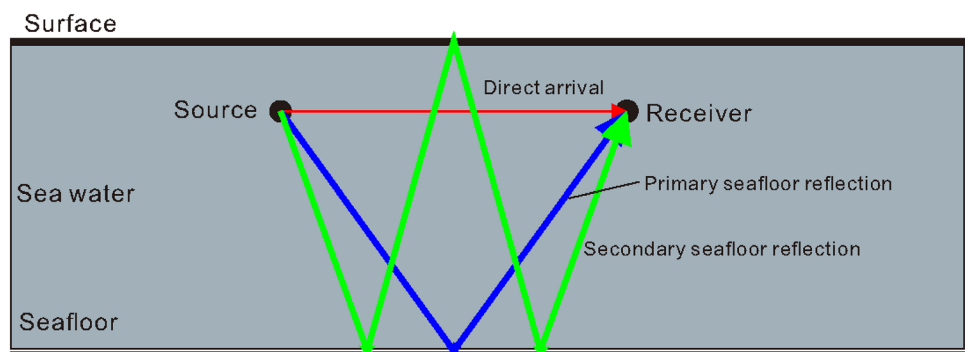
It is relatively easy to obtain the seafloor-reflected wave from seismic data and to deduce the normally incident wave according to the source wavelet and the water depth. However, the seismic record does not directly provide the source wavelet. Here, we deduce the source wavelet of a sparker from the direct wave record. Under the assumption of an omnidirectional sparker source (the energy radiated in each direction is usually different, as described here), the direct wave is most similar to the source wavelet due to the relative homogeneity of seawater, which enhances the possibility to deduce the source wavelet.

Based on the condition that a sparker source is omnidirectional, the seafloor reflection coefficient can be estimated from the primary seafloor reflection and direct wave in the vertical direction:

$$RC = \frac{A_p}{A_d} \times \frac{T_p}{T_d} \tag{4}$$

where  $A_d$  represents the amplitude of the direct wave, and  $T_d$  represents the first arrival time of the direct wave. Note that all terms in Eq. (4) must be of the waves in the

**Fig. 2** Schematic of the ray path of the propagation wave used for calculating the reflection coefficient. Please note that the angle in this picture is arbitrary



normal or vertical direction. The maximum amplitude of both the direct wave and the seafloor-reflected wave in the time domain can be obtained for calculating the reflection coefficient.

The reflection coefficient can also be estimated in the frequency domain:

$$RC(f) = \frac{FS_p(f)}{FS_d(f)} \times \frac{T_p}{T_d} \quad (5)$$

where  $RC(f)$  represents the reflection coefficient spectrum;  $FS_p(f)$  represents the frequency spectrum of the primary seafloor reflection; and  $FS_d(f)$  represents the frequency spectrum of the direct wave. This expression also incorporates an amplitude compensation for spherical spreading.

To reduce the uncertainty in the inversion results, we may present the reflection coefficient by the estimated amplitude data at the optimal frequency of a high signal-to-noise ratio, such as the center frequency:

$$RC(f_c) = \frac{A_p(f_c)}{A_d(f_c)} \times \frac{T_p}{T_d} \quad (6)$$

where  $RC(f_c)$  represents the reflection coefficient calculated according to the amplitude information at the center frequency;  $A_p(f_c)$  represents the amplitude of the primary seafloor reflection at the center frequency; and  $A_d(f_c)$  represents the amplitude of the direct wave at the center frequency.

However, the direct waves recorded in seismic data are usually not recorded in the vertical direction below the source but in the horizontal direction parallel to the source, and the sparker sources employed for seismic exploration usually produce energy with a certain directivity, which means that a certain deviation arises if we treat the sparker source as an omnidirectional seismic source. This energy directivity is designed to improve seismic efficiency, making it a common phenomenon in the field of seismic exploration. Hence, we cannot disregard the energy variation in radiating directions from the sparkers or other seismic sources, although sometimes the direct waves on the raw seismic record are strong enough to cause disbelief. Assuming that the seismic source is stable, we can simply correct Eq. (6) with a constant value (here, we denote this constant value as HTV, namely, the horizontal-to-vertical amplitude ratio):

$$RC(f_c) = \frac{A_p(f_c)}{A_d(f_c)} \times \frac{T_p}{T_d} \times HTV \quad (7)$$

where  $HTV = A_{SWH}/A_{SWV}$ ,  $A_{SWH}$  represents the amplitude of seismic waves traveling in the horizontal direction toward the hydrophones, and  $A_{SWV}$  represents the amplitude of seismic waves traveling in the vertical direction toward the seafloor. We need to determine the HTV constant to estimate

the reflection coefficient. The most direct way is to measure the radiation pattern from HTV of the sparker source, which would be difficult for many existing data. Another way is to calibrate the HTV constant based on some known background information, which is the method applied in this work.

## Results of a case study

### Data sources and assumptions for calculating seafloor reflectivity using marine sparker data

The seismic data employed for the case study were acquired with a marine high-resolution single-channel seismic system that consists of a CSP2200 (a deck unit for the seismic source, produced by Applied Acoustic Engineering), a Squid-2000 (a 120 multi-electrode emission array, produced by Applied Acoustic Engineering), and a Geo-Sense Mini Streamer (a 24-element receiving array with a hydrophone interval of 20 cm, produced by GEO Marine Survey Systems). The seismic source and hydrophone streamer were towed behind the survey ship on opposite sides. The shot interval of the sparker source was 2 s with an average sailing speed of 5 knots; hence, the trace spacing is approximately 6 m. The discharge energy was 1200 J, and the length of the survey line was approximately 35 km.

Since the seafloor acoustic reflectivity varies with the angle of incidence, calculating the reflection coefficient based on reflected seismic data, which assumes normal incidence, is valid only for incidence angles within approximately 15° degrees from the normal (e.g., Bull et al. 1998; Sheriff and Geldart 1995). For single-channel marine seismic data acquired with a sparker source, this information should be considered because the offset between the source and the receiver is too large in comparison with the water depth in coastal areas. For example, with an offset of approximately 10 m, the reflection coefficients should be considered valid for water depths greater than 19 m. Although a single-channel seismic system usually consists of a multi-element array to improve the signal-to-noise ratio, this arrangement is not considered in the calculation in this paper.

In addition to all previously mentioned assumptions, we also disregard the absorption of acoustic waves, including the reflection loss in seawater. Thus, for calculating the seafloor reflection coefficient from the direct wave and primary seafloor reflection, we consider only the effect of spherical spreading (the directivity of the sparker source is discussed based on the calculation results), which can be corrected via amplitude compensation according to the travel time.

## Data preprocessing

### Arrival time picking of the direct wave and seafloor reflection

Picking the arrival times of the direct and seafloor reflection waves is the first major step in calculating the reflection coefficient. First, we select the reference trace and define the reference direct wave sequence according to the threshold for the field data. The threshold is denoted by the sampling numbers in the process of the algorithm implementation. Second, we correlate each recorded trace with the reference direct wave, to pick the arrival time of the direct wave for each trace according to the correlation results. This process can be implemented in a specific section to improve the processing efficiency and accuracy. For example, for the seismic data shown in Fig. 3, we implement the arrival time selection of the direct waves in the first 20 milliseconds.

Since the sparker source is repeatable, the source wavelet should be similar between different shots along the same seismic line. However, because the acoustic signature of the sparker sources is influenced by the dynamics or property changes in the seawater, the picking results of arrival time should be checked carefully.

Using the selected direct wave and its arrival times, we can build a statistical direct wave; we name it the estimated source wavelet. We can then obtain the arrival times of the seafloor reflection via the correlation method, using the estimated source wavelet. Similarly, we can determine the arrival times of the seafloor reflections in another selected section. For example, for the seismic data shown in Fig. 4, we can implement the arrival time selection of the seafloor reflections in the section between 20 milliseconds and 120

milliseconds. Note that the seismic data displayed in Fig. 3 are the first 100 traces in Fig. 4.

However, many factors could have influenced the results, such as shallowly buried bedrock or shallow gas. Hence, we should improve the results based on the practical situation. Median filtering, which is applied here, is an effective means for this problem because the seafloor usually changes steadily. The picking results of the arrival times of the direct waves and the primary and secondary seafloor reflections are displayed in the seismic profile in Fig. 4.

According to the previous description, calculating the normal seafloor reflectivity from reflection seismic data is valid for incidence angles within  $15^\circ$  from the vertical. According to the arrival time results of the direct waves and setting the acoustic velocity of seawater to 1500 m/s, the minimum offset between the source and the receiver is 6.0 m, while the maximum offset is 10.2 m. For the minimum offset, the minimum valid water depth is 7.73 m, and the corresponding two-way travel time is 10.30 ms. For the maximum offset, the minimum valid water depth for the reflection coefficient calculation is 19.03 m, and the corresponding two-way travel time is 26.27 ms. Hence, all of the seismic traces shown in Fig. 4 are valid for the reflection coefficient calculation.

### QC for the source wavelet

Quality control (QC) of data is usually necessary for seismic data inversion and is an important part for resolving the uncertainty in inversion results. In this work, the first step of QC can be implemented by selecting data for spectrum analysis and for reflection coefficient calculation. According to the previous description regarding marine sparker

**Fig. 3** Direct wave record in marine single-channel seismic data, which shows the primary pulse and its water surface reflection in the red dashed window, and the bubble pulse and its water surface reflection in the blue dashed window

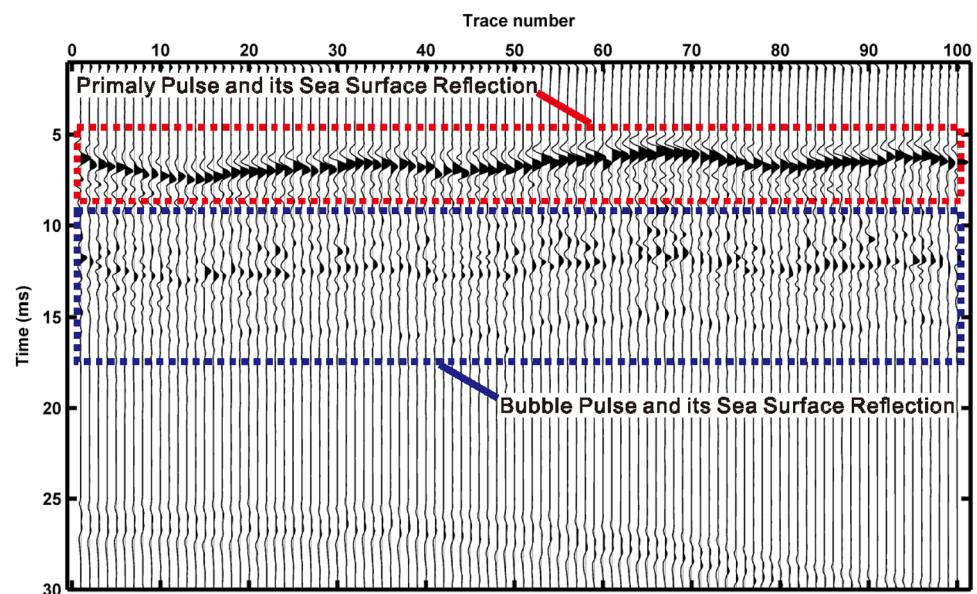
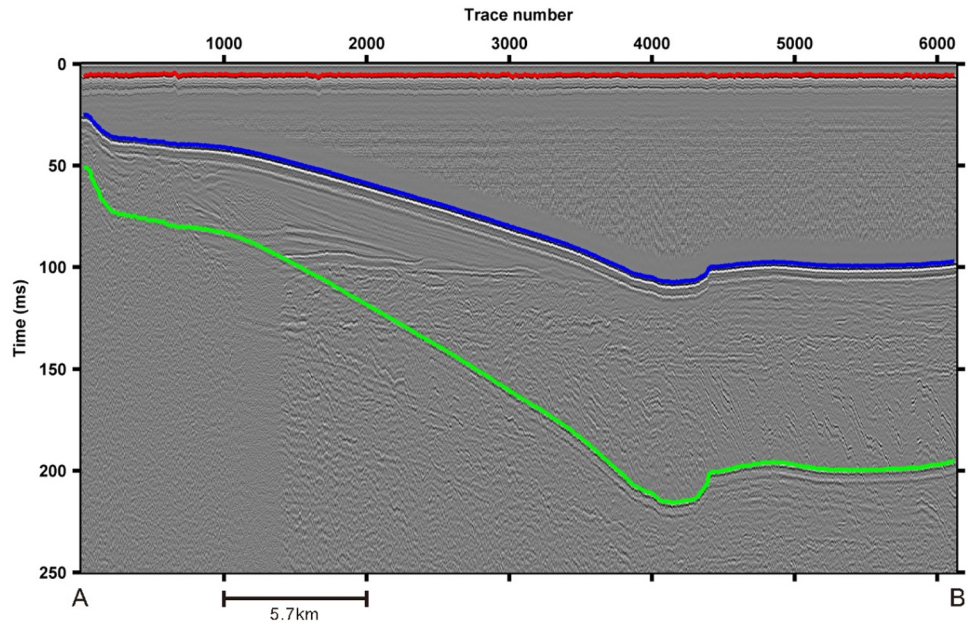


**Fig. 4** Time picks of the direct wave (red curve), the primary seafloor reflection (blue curve), and the secondary seafloor reflection (green curve), respectively

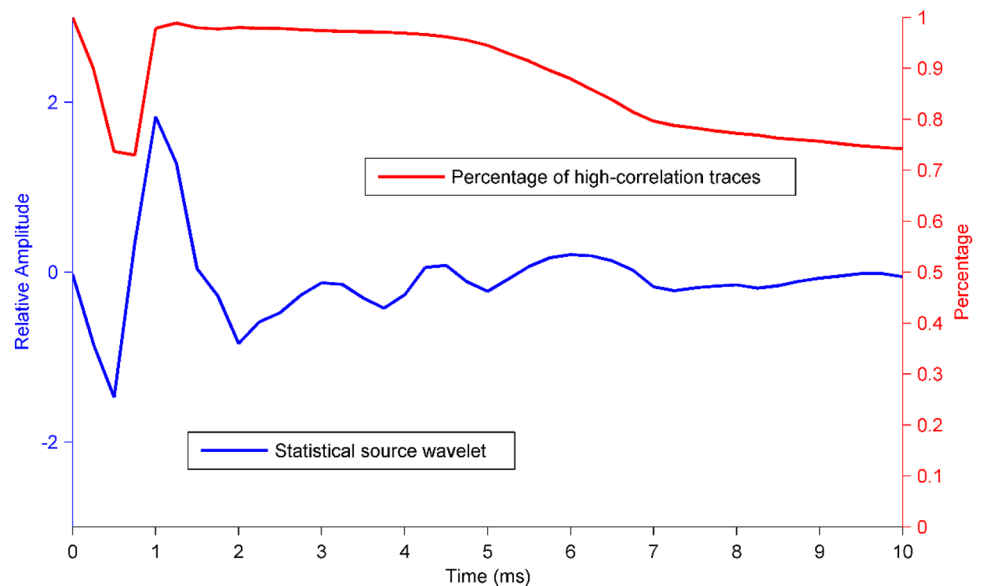


sources, the acoustic signature includes the primary pulse generated by the underwater discharge, the bubble pulses generated by bubble collapse, and their reflections from the sea surface. Based on the arrival time picking results of the direct waves, we can calculate the correlation coefficient of the waveform between the estimated source wavelet and the direct wave record in each trace. By changing the threshold of the duration of the direct wave, we can calculate the correlation coefficients for different time durations.

Figure 5 shows the estimated source wavelet and the percentage of high-correlation traces as function of time, based on the seismic data displayed in Fig. 4. Note that the percentage of high-correlation traces changes with the duration

threshold from 1 sample to 41 samples (10 ms). As shown in Fig. 5, the proportion of highly correlated traces (with a minimum correlation coefficient of 0.8) decreases with increasing computation length, revealing the instability of bubble pulses and their reflections from the sea surface, as discussed in the introduction. More than 90% of the direct waves recorded in seismic traces have a high correlation coefficient with the estimated source wavelet in the first 5 ms, indicating that the acoustic signature of the source is relatively stable. Considering the physical process of underwater discharge, we select the first 1.5 ms from the arrival time for the seafloor reflectivity calculation, which includes

**Fig. 5** Percentage of high-correlation traces changes as a function of the time duration threshold



the primary pulse and its sea surface reflection. Refer to the latter part for the results.

**QC for the seismic traces**

Using the arrival time of the seafloor reflection and the length of the source wavelet that we have determined, we can conduct a spectrum analysis of the seafloor-reflected waves after the spherical spread amplitude compensation. The analysis results in Fig. 6 show the energy characteristics of the seafloor-reflected waves in both the frequency and the spatial domains. The characteristics in the frequency domain depend mainly on the seismic source,

while the characteristics in the spatial domain depend predominantly on the physical properties of the seafloor. As shown in Fig. 6, the seafloor reflectivity near the B-end is stronger than that near the A-end.

However, due to the complex variability in the marine environment, echoes from the seafloor are affected by many factors. Before calculating the seafloor reflection coefficient, we selected the seismic traces involved in the calculation according to the results of the correlation analysis between the direct wave and the seafloor reflection. The seafloor reflection in the seismic record is the response of an acoustic wave to the seafloor, including reflection and volume scattering, which are beyond the scope of this work.

**Fig. 6** Spectrum analysis of the seafloor reflections

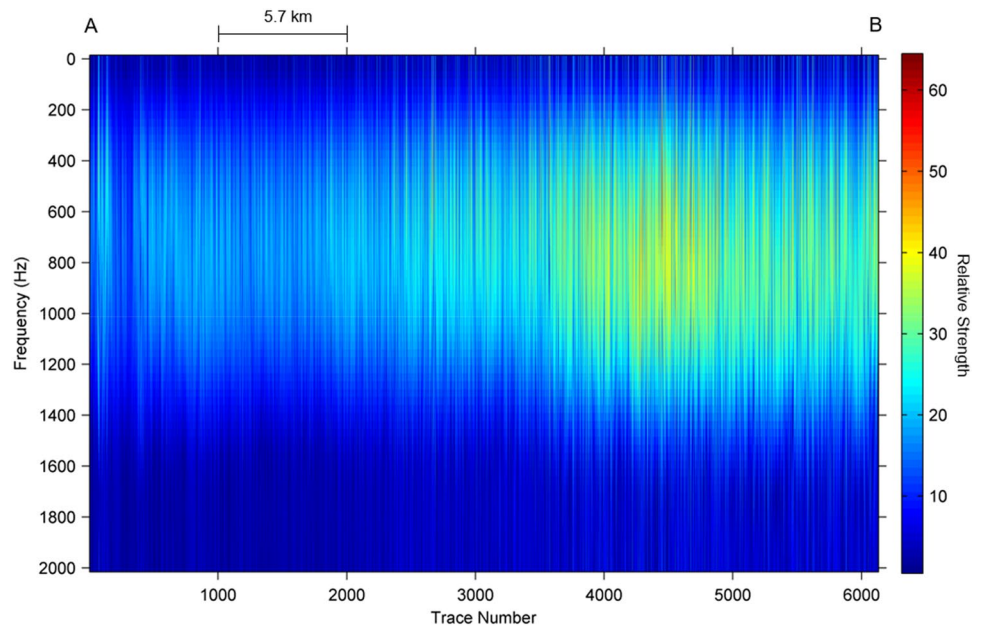


**Fig. 7** Correlational results of the deduced direct wave and seafloor reflection

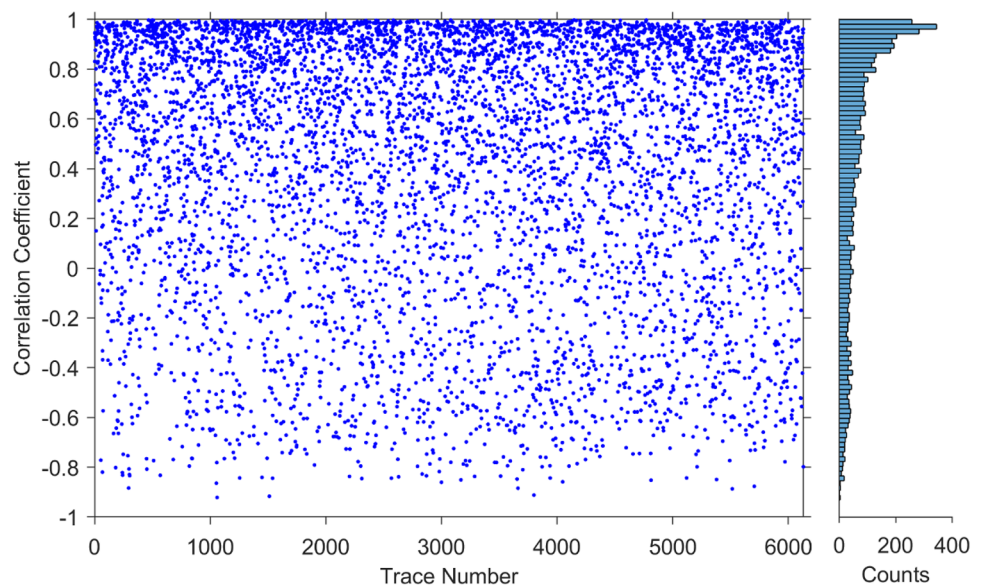


Figure 7 presents the results of the correlation analysis of waveforms between the direct waves and the seafloor reflection. The results show that seafloor reflection and direct waves have a wide range of correlation values. The distribution of the results is relatively similar in the horizontal direction, indicating that there are some other random factors that have not been considered. However, the distribution is not uniform in the vertical direction. We divided the correlation coefficient into 100 sections and counted the number of traces in each section, as shown in the histogram on the right side of Fig. 7. The correlation coefficients of approximately one-third of all seismic traces exceed 0.8. In the following work, we use only the seismic traces with a high correlation coefficient (greater than 0.8).

### Reflection coefficient calculation

Based on the picking results for the primary and secondary seafloor reflections, the seafloor reflection coefficients can be calculated using Eq. (1). However, as previously mentioned, the recorded signals at the two-way travel time of the secondary seafloor reflection contain multiple waves, additional reflectors and background noise. For instance, we select the records of the traces between No. 5000 and No. 6000 and the records for the two-way travel time between 160 and 260 ms, which mainly include the records near the secondary seafloor reflection, as shown in Fig. 8. The selected part corresponds to an area where the seafloor is relatively flat.

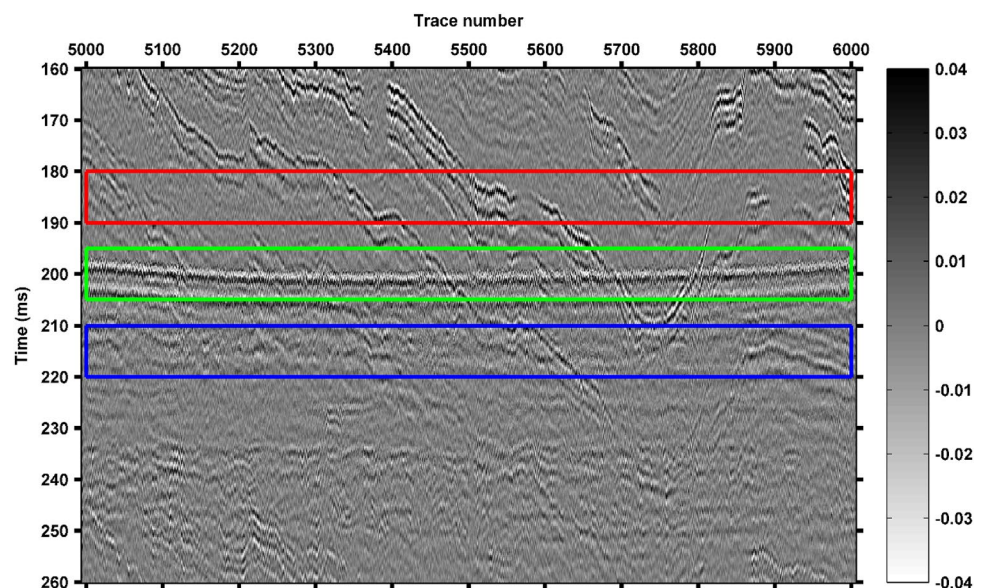
We select three new time windows in the profile, with the same traces from No. 5000 to No. 6000. The first window has two-way travel times between 180 and 190 ms. The second window has two-way travel times between 195 and 205 ms, which includes the secondary seafloor reflection. The third window has two-way travel times between

210 and 220 ms. The three windows are also present on the seismic profile shown in Fig. 8. We separately performed a spectrum analysis for the trace records in each selected window and calculated the mean amplitude spectrum of all traces in their respective windows. The results are shown in Fig. 9.

Figures 8 and 9 indicate that the reflected waves from the underground strata are comparable with secondary seafloor reflection. According to Fig. 9, the records (in green window) around the travel time of the secondary seafloor reflection seem to be dominated by the reflectors of underground strata, of which the main frequency band nears the low-frequency end. Hence, the secondary reflections should be separated from the strata reflections if we want to acquire the seafloor reflection coefficients using primary and secondary reflected waves. However, this goal is unrealistic since the strata reflections comprise the target of seismic exploration and are usually unpredictable.

Since we did not calibrate the seismic source before conducting the survey work to obtain the difference in the energy radiated by it in the vertical and horizontal directions, we have to use Eq. (6) instead of Eq. (7) to calculate the reflection coefficients. Based on Eq. (6), it is possible to calculate the seafloor reflection coefficient in the light of primary seafloor reflection and direct wave record. According to the spectrum analysis of the direct wave, seafloor reflection and background noise, the background noise is insignificant (for these raw seismic data, the magnitude of the background noise is approximately 2% of the seafloor reflection in the deep water); hence, it is disregarded here when calculating the seafloor reflection coefficient. The calculation results are given in Fig. 10, which are dimensionless parameters. However, a part of the calculated reflection coefficients is greater than 1, which is not in accordance with

**Fig. 8** Seismic profile showing the selected traces from No. 5000 to No. 6000 and three colored windows





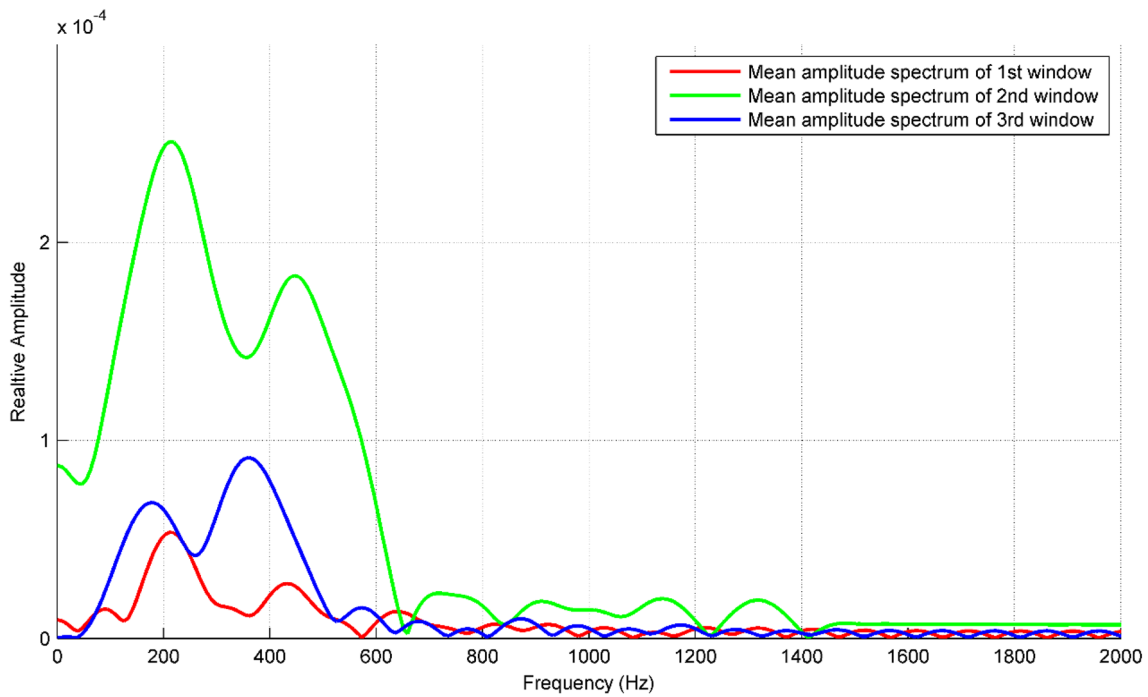
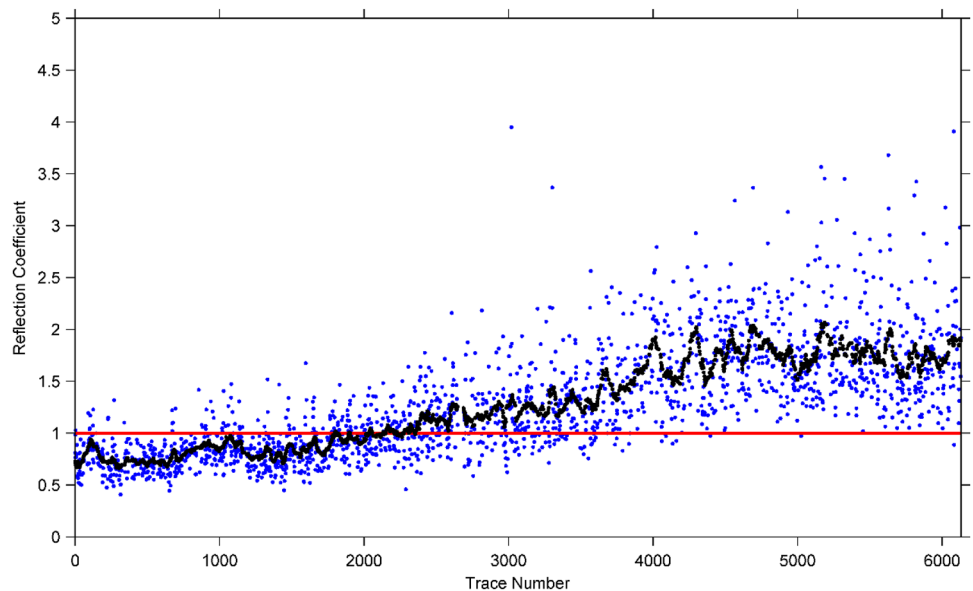


**Fig. 9** Spectral analysis of the selecting windows near the secondary seafloor reflection

**Fig. 10** Reflection coefficients calculated using the primary seafloor reflection and direct wave data (based on amplitudes at the center frequency of 593 Hz). Each of the average values (black dots) is calculated based on 21 traces in the neighborhood



the physical definition. These unusual phenomena will be discussed in the next section.

**Seafloor reflectivity and surface sediment**

The survey line employed for this case study is located along the west part of the Taiwan Strait. It is worth noting that we have conducted some work on the same survey line

position based on Chirp data. The results show that the grain size characteristics of the sediment have a significant corresponding relationship with the reflection coefficient. According to previous studies of this region (e.g., Fang et al. 2012; Liu et al. 2008; Xu et al. 2009), the sediment characteristics are governed by submarine topography, tidal action, river transport from the Chinese mainland and Taiwan Island, the Kuroshio branch, the South China

Sea warm current, and the East China Sea circulation. The survey line location can be viewed in our previous work (Zheng et al. 2019).

Considering that some of the calculated seafloor reflection coefficients here are greater than 1 (which is physically impossible), we denote the estimated seafloor reflectivity in decibels as the *uncorrected echo intensity* ( $UEI = 20 \times \log_{10} RC_{uncorrected}$ ) to prevent confusion with terms commonly employed in the literature, as shown in Fig. 11. Practically, the results can be smoothed for analyzing the acoustic properties of seafloor sediments on large scales. The black dots in Fig. 10 and the results shown in Fig. 11 present the smoothed results of 21 traces (approximately 360 m in the spatial domain). There are four types of main sediments in four spatial zones separated by the black vertical lines, as shown in Fig. 11. To compare the results of the two methods described earlier, we also calculated the UEI based on the primary and secondary seafloor reflections, as shown in Fig. 11. Without the results of geological sampling, it would be difficult for us to judge the authenticity of the two calculation results. Nevertheless, we find that the results calculated based on the primary seafloor reflection and direct wave are more in line with our perception.

According to the sampling and analysis results, the seismic line in this example spans the types of subsea sediments of clayey silt, silt, sandy silt and silty sand from the shore to the sea. In general, according to the results calculated based on the primary seafloor reflection and direct wave data, fine particles correspond to lower echo intensities, whereas coarse particles correspond to higher echo intensities. This correspondence is consistent with our previous perception. However, we do not observe this correspondence in the results calculated based on the primary and secondary

seafloor reflection data. The reasons for this phenomenon have been analyzed earlier when describing the calculation method; that is, the secondary reflection is “contaminated” by the additional reflectors from the strata below the seafloor.

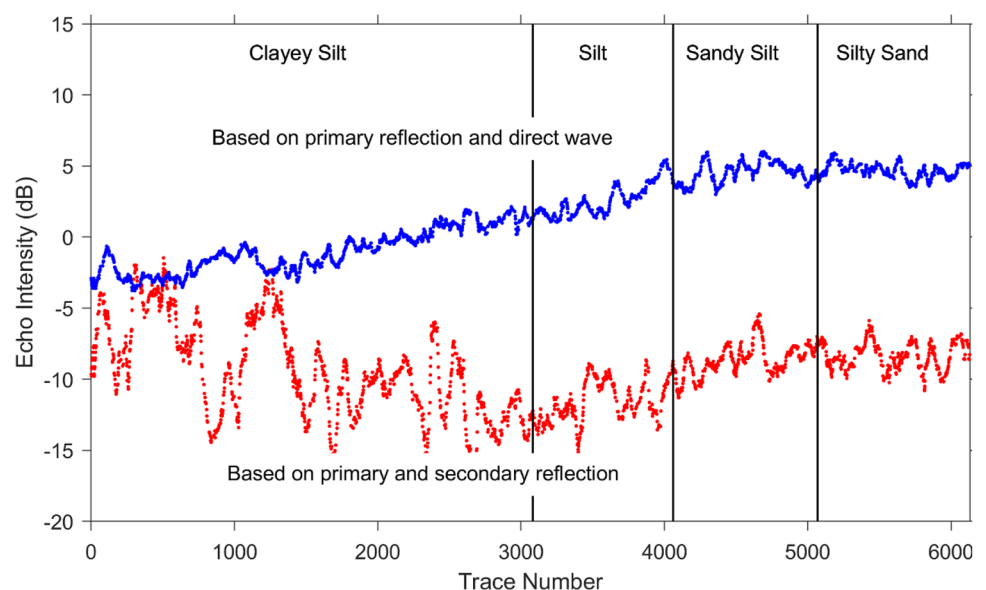
There are, however, many fluctuations along the survey line, as shown in both Figs. 10 and 11. It is worth noting that the sediment type is defined by the various sediment components, and the geological sampling stations are very sparse in comparison with the spatial sampling interval of the seismic survey. Hence, the information reflected by the geological sampling and acoustic inversion actually have similarities, such as the physical properties of seafloor sediments, and some differences, such as changes in spatial scale.

## Discussion

Although seafloor reflectivity is a simple concept, the physical process is not simple. To guarantee a reliable inversion result, we must determine the source signature before estimating the seafloor reflectivity based on seismic data of a sparker source or other types of sources. Unlike chirp sources, sparker sources can be treated as omnidirectional to some extent. Although there may be a significant level of directional variation in the sparker source energy, as noted in this study, it is possible to deduce the source wavelet from the direct wave record under the assumption of homogeneous seawater. The nearly vertically traveling incident wave into the seafloor can be deduced based on the horizontally traveling direct wave and combined with the seafloor reflection to calculate the seafloor reflection coefficient.

Based on the working mechanism of the sparker source, the source signature of the underwater discharge includes a

**Fig. 11** Estimated UEIs using the primary seafloor reflection and direct wave data in comparison with those using the primary and secondary seafloor reflection data. The calculation is also based on amplitudes at the center frequency of 593 Hz. The black dots represent the averaged results of 21 traces



primary pulse, bubble pulses and the associated sea surface reflections. The bubble pulses and associated surface reflection usually act as noise because they are unstable. Hence, they must be excluded from the estimated source wavelet. Considering the stability of the source signal, it is reasonable to select the wavelength based on the correlation results of waveforms between direct waves and the estimated source wavelet for reflection coefficient computation.

The seafloor reflection coefficient, which is estimated based on direct waves and seafloor reflections, are referred to as the UEI in the case study to distinguish it from the real seafloor reflectivity. Following previous studies (e.g. Hamilton 1970; LeBlanc et al. 1992; Zheng et al. 2012), our data preprocessing results show that marine sediment types can be classified based on the UEI deduced from the sparker data. However, before applying this relationship to more practical works, additional research is necessary to calibrate the results similar to those shown in Figs. 10 and 11.

Based on the results in this study, the acoustic wave energy emitted by the sparker source in the vertical direction is greater than that emitted in the horizontal direction, which is consistent with the design concept of the seismic source. According to the analysis in the “Data preprocessing” section, we assume that the source wavelet is stable, namely, with a constant ratio of the acoustic intensity radiated in the horizontal direction toward the hydrophones to the acoustic intensity radiated vertically downward. In these circumstances, we can calibrate the HTV constant in Eq. (7) according to some published data. For instance, according to Hamilton (1970), the reflection coefficient of silty sand is 0.3228 (−9.9 dB). Hence, we can calibrate the HTV based on the calculated reflection coefficients between Trace 5069 and Trace 6131 (averaging, equal to 1.7671), which corresponds to the bottom type of silty sand. The HTV in this work is equal to 0.1827, indicating that the sparker source exhibits strong directivity. The intensity of a direct wave is less than 20% of that of the wave that is propagated vertically downward. Hence, the value range of the vertical axis of Fig. 10 should range from 0 to 0.9135.

When acoustic waves interact with the seafloor, the interaction produces not only reflected and transmitted waves but also various types of scattering due to the roughness of the water-sediment interface, spatial variations of the physical properties of sediments, and discrete inclusions such as shell fragments or bubbles (Jackson and Richardson 2007). Hence, the echo from the seafloor is the combined result of reflection and scattering. For the corresponding wavelength at the center frequency of the acoustic wave emitted by the sparker source, we believe that the contribution of seafloor scattering to the echo is not negligible. Hence, a measurement of the radiation pattern from horizontal to vertical should be conducted to obtain more valuable results. Because it is very difficult to quantify the contributions of

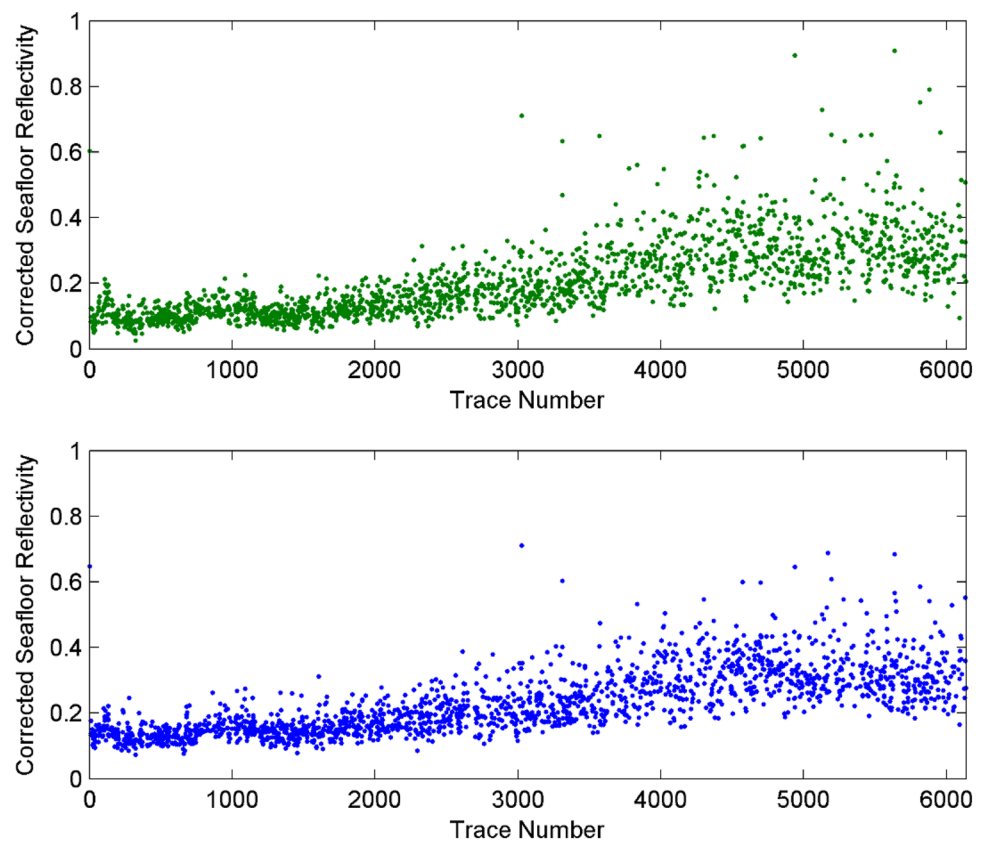
reflection and scattering to the echo, in this work, we use the estimated effect of the two to assess some acoustic characteristics of the seafloor.

Figure 10 shows that the calculated results are more dispersive on the right side than those on the left side. We speculate that this pattern is related to the particle size of the seafloor sediments. As shown in Fig. 11, the parts near the left end correspond to fine seafloor sediments, while the parts near the right end correspond to coarse seafloor sediments. The former has higher clay contents; hence, the texture is softer and corresponds to a lower seafloor reflectivity. The latter consists of mainly coarse particles such as sands; hence, the texture is harder with a higher seafloor reflectivity. In addition, the coarse sediment is able to produce more significant scattering, which is more randomly influences the seafloor reflection and results in the dispersibility of the calculated seafloor reflectivity. We also compare the seafloor reflectivities deduced from chirp data with those from sparker data, but we do not perform a comparison with the results in this work since relevant studies have shown that seasonal changes and typhoon activity influence the seafloor reflectivity (Wood et al. 2014; Yang et al. 2016), especially in nearshore shallow water. In particular, our study area is severely affected by typhoon activity. Furthermore, we lack reliable analysis results of sediment cores to explain the difference between the two data inversion results. However, the corresponding relationships between the sediment type and seafloor reflectivity derived from the chirp data and sparker data are consistent.

As mentioned in the “Methods” section, we can also calculate the seafloor reflectivity based on the maximum amplitude of both the direct wave and the seafloor-reflected wave in the time domain. The results are similar to the previously presented calculations based on the amplitude information at the center frequency shown in Fig. 12; both of the calculations are corrected according to the results of the previous discussion. However, there are two points that need to be declared: the calculated results in the time domain contain one point greater than 1 and one point less than 0, which are not shown in the picture. For the parts near the right end, the calculation results based on the maximum amplitude in the time domain are more scattered than those deduced in the frequency domain, which can be more easily observed on the decibel scale. The calculation in the frequency domain can also provide the reflectivity spectrum, which can be applied to further investigate the seafloor reflectivity in a wide frequency band. However, these studies need further work.

The inversion results of the sparker data can provide the response characteristics of seafloor to acoustic signals in the frequency band of hundreds of hertz. Although this work does not report the calculation results of the reflection coefficient spectrum, it is easy to obtain the corresponding results according to the above procedure and Eq. (5). The reflection

**Fig. 12** Comparison of the seafloor reflectivities calculated in time domain (upper plot) and frequency domain (lower plot)



coefficient spectrum would help to study the relationship between the sediments and the frequency of the acoustic signal. It is possible to carry out the acoustic inversion of sparker data in deeper strata. However, to fully utilize the seafloor reflectivity inversion based on the direct wave and seafloor reflections of sparker data, we need to calibrate the energy relationship between the seismic wave propagating downward and the direct wave.

## Conclusions

This work presents a detailed procedure for calculating the seafloor reflection using the direct and seafloor reflection waves of sparker data. We obtain the wavelet of sparker source using the direct wave data and estimate the incident wave at the seafloor using the source wavelet and water depth. The seafloor reflectivity (UEI) is computed using the reflected wave and estimated incident wave at the seafloor. We observed a significant difference in the acoustic wave energy radiated by the sparker source in the horizontal and vertical directions, which should be considered during the inversion process.

The source signature of the sparker is determined by the primary pulse, bubble pulses and sea surface reflections of these pulses. Because the bubble pulses are unstable, we

calculate the seafloor reflectivity using only the primary pulse and its surface reflections. The case study shows agreement between the seismic calculations and the geological data, indicating the possibility of using the seafloor reflectivity deduced from sparker data for acoustic classification of bottom sediment, although the estimated results still need to be calibrated with the energy directionality of the sparker source.

**Acknowledgements** This work was supported by the National Natural Science Foundation of China (No. 41230318). We thank Aijun Wang and Jianyong Fang for providing the geological data. We also thank the reviewers for their valuable suggestions.

## References

- Breslau LR (1964) An acoustic surveying technique for determining sea-floor sediments. 939–950
- Bull JM, Quinn R, Dix JK (1998) Reflection coefficient calculation from marine high resolution seismic reflection (Chirp) data and application to an archaeological case study. *Mar Geophys Res* 20:1–11
- Buogo S, Plocek J, Vokurka K (2009) Efficiency of energy conversion in underwater spark discharges and associated bubble oscillations: experimental results. *Acta Acust United Acust* 95:46–59
- Chiu LYS, Chang A, Lin Y-T et al (2015) Estimating geoacoustic properties of surficial sediments in the North Mien-Hua canyon region with a Chirp sonar profiler. *IEEE J Ocean Eng* 40:222–236

- Chotiros NP, Lyons AP, Osler J et al (2002) Normal incidence reflection loss from a sandy sediment. *J Acoust Soc Am* 112:1831–1841
- Cook JA, Gleeson AM, Roberts RM et al (1997) A spark-generated bubble model with semi-empirical mass transport. *J Acoust Soc Am* 101:1908–1920
- Dettmer J, Dosso SE, Holland CW (2007) Uncertainty estimation in seismo-acoustic reflection travel time inversion. *J Acoust Soc Am* 122:161–176
- Dettmer J, Dosso SE, Holland CW (2009) Model selection and Bayesian inference for high-resolution seabed reflection inversion. *J Acoust Soc Am* 125:706–716
- Dettmer J, Holland CW, Dosso SE (2013) Transdimensional uncertainty estimation for dispersive seabed sediments. *Geophysics* 78:WB63–WB76
- Duchesne MJ, Bellefleur G, Galbraith M et al (2007) Strategies for waveform processing in sparker data. *Mar Geophys Res* 28:153–164
- Endler M, Endler R, Bobertz B et al (2015) Linkage between acoustic parameters and seabed sediment properties in the south-western Baltic Sea. *Geo-Mar Lett* 35:145–160
- Faas RW (1969) Analysis of the relationship between acoustic reflectivity and sediment porosity. *Geophysics* 34:546–553
- Fang J, Chen J, Wang A et al (2012) The distribution characteristics of grain size and mineral of surface sediment in the Taiwan Strait. *Acta Oceanol Sin* 34:91–99
- Hamilton EL (1970) Reflection coefficients and bottom losses at normal incidence computed from pacific sediment properties. *Geophysics* 35:995–1004
- Hastrup OF (1969) Digital analysis of acoustic reflectivity in the Tyrhenian Abyssal Plain. *J Acoust Soc Am* 47:181–190
- Heard GJ (1997) Bottom reflection coefficient measurement and geoacoustic inversion at the continental margin near Vancouver Island with the aid of spiking filters. *J Acoust Soc Am* 101:1953–1960
- Holland CW, Dosso SE (2013) Mid frequency shallow water fine-grained sediment attenuation measurements. *J Acoust Soc Am* 134:131–143
- Hou Z, Chen Z, Wang J et al (2018) Acoustic impedance properties of seafloor sediments off the coast of Southeastern Hainan, South China Sea. *J Asian Earth Sci* 154:1–7
- Huang Y, Yan H, Wang B et al (2014) The electro-acoustic transition process of pulsed corona discharge in conductive water. *J Phys D* 47:255204–255201
- Huang Y, Zhang L, Yan H et al (2016) Experimental study of the electric pulse-width effect on the acoustic pulse of a plasma sparker. *IEEE J Oceanic Eng* 41:724–730
- Huang Y, Zhang L, Zhang X et al (2015) Electro-acoustic process study of plasma sparker under different water depth. *IEEE J Oceanic Eng* 40:947–956
- Jackson DR, Richardson MD (2007) High-frequency seafloor acoustics. Springer, New York
- Kibblewhite AC (1989) Attenuation of sound in marine sediments: A review with emphasis on new low-frequency data. *J Acoust Soc Am* 86:716–738
- Kim DC, Kim GY, Yi HI et al (2012) Geoacoustic provinces of the South Sea shelf off Korea. *Quatern Int* 263:139–147
- LeBlanc LR, Mayer L, Rufino M et al (1992) Marine sediment classification using the chirp sonar. *J Acoust Soc Am* 91:107–115
- Liu JP, Liu CS, Xu KH et al (2008) Flux and fate of small mountainous rivers derived sediments into the Taiwan Strait. *Mar Geol* 256:65–76
- Liu Y, Liu X, Ning H (2016) Analysis and improvement for a linearized seafloor elastic parameter inversion method. *J Appl Geophys* 128:110–114
- Liu Y, Zhong Y, Liu K et al (2020) Seafloor elastic-parameter estimation based on a regularized AVO inversion method. *Mar Geophys Res* 41:1–11
- Parrott DR, Dodds DJ, King LH et al (1980) Measurement and evaluation of the acoustic reflectivity of the sea floor. *Can J Earth Sci* 17:722–737
- Rakotonarivo S, Legris M, Desmare R et al (2011) Forward modeling for marine sediment characterization using chirp sonars. *Geophysics* 76:T91–T99
- Schock SG (2004a) A method for estimating the physical and acoustic properties of the sea bed using chirp sonar data. *IEEE J Oceanic Eng* 29:1200–1217
- Schock SG (2004b) Remote estimates of physical and acoustic sediment properties in the South China Sea using chirp sonar data and the Biot model. *IEEE J Oceanic Eng* 29:1218–1230
- Schock SG, Leblanc LR, Mayer LA (1989) Chirp subbottom profiler for quantitative sediment analysis. *Geophysics* 54:445–450
- Sheriff RE, Geldart LP (1995) *Exploration Seismology*. Cambridge University Press, Cambridge
- Smith DT, Li WN (1966) Echo-sounding and sea-floor sediments. *Mar Geol* 4:353–364
- Stevenson IR, Mccann C, Runciman PB (2002) An attenuation-based sediment classification technique using Chirp sub-bottom profiler data and laboratory acoustic analysis. *Mar Geophys Res* 23:277–298
- Stoll RD, Kan T-K (1981) Reflection of acoustic waves at a water–sediment interface. *J Acoust Soc Am* 70:149–157
- Tian Y, Chen Z, Hou Z et al (2019) Geoacoustic provinces of the northern South China Sea based on sound speed as predicted from sediment grain sizes. *Mar Geophys Res* 40:571–579
- Tseng Y-T, Ding J-J, Liu C-S (2012) Analysis of attenuation measurements in ocean sediments using normal incidence Chirp sonar. *IEEE J Oceanic Eng* 37:533–543
- Tyce RC (1976) Near-bottom observations of 4 kHz acoustic reflectivity and attenuation. *Geophysics* 41:673–699
- Vardy ME (2015) Deriving shallow-water sediment properties using post-stack acoustic impedance inversion. *Near Surface Geophysics* 13:143–154
- Vardy ME, Vanneste M, Henstock TJ et al (2017) State-of-the-art remote characterization of shallow marine sediments: the road to a fully integrated solution. *Near Surf Geophys* 15:387–402
- Wan L, Zhou J-X, Rogers PH (2010) Low-frequency sound speed and attenuation in sandy seabottom from long-range broadband acoustic measurements. *J Acoust Soc Am* 128:578–589
- Wang J, Guo C, Liu B et al (2016) Distribution of geoacoustic properties and related influencing factors of surface sediments in the southern South China Sea. *Mar Geophys Res* 37:337–348
- Wood WT, Martin KM, Wooyeol J et al (2014) Seismic reflectivity effects from seasonal seafloor temperature variation. *Geophys Res Lett* 41:6826–6832
- Xu K, Milliman JD, Li A et al (2009) Yangtze- and Taiwan-derived sediments on the inner shelf of East China Sea. *Cont Shelf Res* 29:2240–2256
- Yang G-B, Lu L-G, Wang G-S et al (2016) Coastal sound-field change due to typhoon-induced sediment warming. *J Acoust Soc Am* 140:EL242–E246
- Zheng H-b, Yan P, Chen J et al (2012) Seabed sediment classification in the northern South China Sea using inversion method. *Appl Ocean Res* 39:131–136
- Zheng J, Xu J, Tong S et al (2019) The significance of seabed reflection coefficient derived from high frequency seismic data to marine sedimentary environment. In: Tang W (ed) *IOP Conference Series: Earth and Environmental Science*. IOP Publishing, Shanya